Chemical Engineering Journal 428 (2022) 131946

Contents lists available at ScienceDirect

Chemical Engineering Journal

journal homepage: www.elsevier.com/locate/cej

Re-evaluating adsorbed and free methane content in coal and its ad- and desorption processes analysis

Yong Li [a,*], Zhuangsen Wang [a], Shuheng Tang [b], Derek Elsworth [c]

[a] State Key Laboratory of Coal Resources and Safe Mining, College of Geosciences and Surveying Engineering, China University of Mining and Technology, Beijing 100083, China
[b] School of Energy Resources, China University of Geosciences, Beijing 100083, China
[c] Department of Energy and Mineral Engineering, Geosciences, EMS Energy Institute and the G3 Center, Pennsylvania State University, University Park, PA 16802, USA

ARTICLE INFO

Keywords:
Gas phases
Coalbed methane
Adsorption capacity
Isothermal adsorption

ABSTRACT

Discriminating methane mass stored between free and adsorbed states in coal and shale is crucial in devising optimal gas recovery strategies and greenhouse control. Existing methods of estimating free and adsorbed gas contents in core plugs cannot fully discriminate between methane phases due to high levels of compaction and the resulting complex architecture of micropores. We propose a method using nuclear magnetic resonance (NMR) spectroscopy to define adsorbed/free methane ratios in powdered coal at pressures up to 15 MPa and to verify its fidelity against standard isothermal adsorption measurements. The methane T_2 spectra exhibit four distinct peaks in the intervals 0.01–1, 1–20, 20–100, and ~ 1000 ms, respectively. The three peaks located < 100 ms all correspond to surface relaxation indicating the presence of adsorbed (0.01–1 ms) and free (1–100 ms) methane. The free methane can be interpreted as occupying both small (1–20 ms) and large (20–100 ms) pores as indicated by relaxation times and their pressure-dependency. The adsorption capacity generally reaches a maximum at ~ 10 MPa with free methane content only lower than adsorbed content below ~ 5 MPa. Adsorbed/free methane ratios recovered by NMR compare favorably with isothermal adsorption results with NMR also capable of calibrating absolute adsorbed methane contents.

1. Introduction

Precise estimation of in-situ gas content in coal and shale is important in resource evaluation and in optimizing recovery strategies [1–3]. However, no routine tests currently exist to distinguish between free and adsorbed gas contents under subsurface conditions. There are several issues related to the estimation of methane content in coal and its modes of storage. First, methane explosions remain a threat to safe mining operations where rates of desorption may lead to outburst and explosion [4]. Second, precise measurement of in-situ methane content is important in the design of effective well drainage systems for methane management to maximize recovery of the large mass stored in the adsorbed state [5,6]. Third, coal seams are a potential choice for carbon sequestration and greenhouse gas control, where storage capacities and modes of security are key controlling parameters [7–10]. Thus, precisely defining methane contents and modes of storage are significant for both resource recovery and CO_2 storage.

Methane is generated during the thermal evolution and coalification processes, with a fraction retained as “unconventional” reserves and the remainder migrating to adjacent traps as “conventional” reserves [5,11–13]. Retained methane is present in adsorbed (on the pore surfaces), free (in the pore or fracture volume) and dissolved (both in oil and water) forms [14,15]. The methane content in coal typically varies from 0.5 m^3/t in lignite to as much as 30 m^3/t in anthracites [3,16,17]. The majority of methane in coal is typically present in the adsorbed state, accounting for>90% of the total methane content [18]. However, losses during coring and recovery render precise estimates of in situ contents unreliable [19] – in particular reducing, readily-lost, and free gas contents. Such losses during sampling may be significant, as suggested by recovery rates from some coalbed methane wells (e.g. in the Qinshui Basin, China) exceeding 100% of that predicted. Similarly, high free gas contents are also observed in coalbed methane wells in the Black Warrior (Alabama), San Juan (New Mexico, Utah, and Colorado) and Powder River (primarily Wyoming) basins [20]. However, presently, there are still no routine methods for the measurement of the proportions of free to adsorbed gas.

* Corresponding author.
E-mail address: liyong@cumtb.edu.cn (Y. Li).

https://doi.org/10.1016/j.cej.2021.131946
Received 15 June 2021; Received in revised form 13 August 2021; Accepted 17 August 2021
Available online 22 August 2021

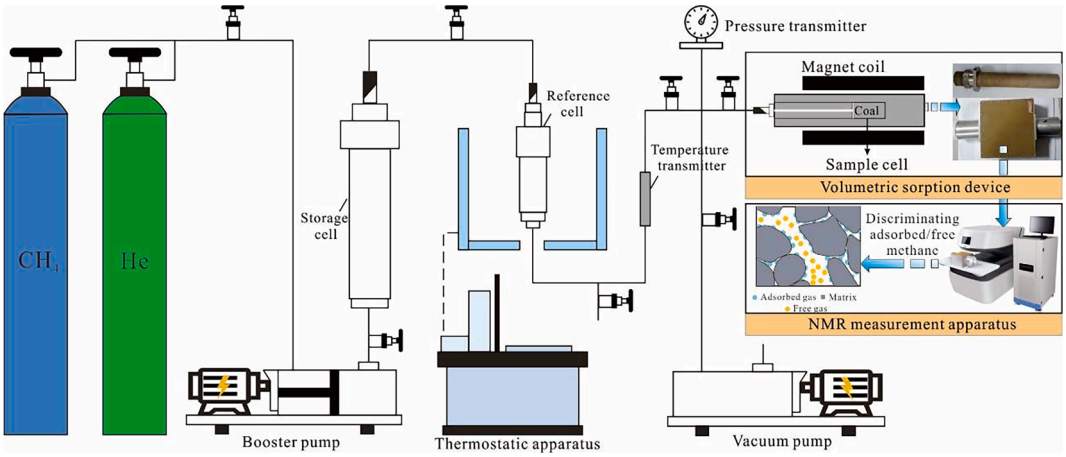

Fig. 1. Low-field NMR setup for measuring methane phases within coal.

The methane content within coal is influenced both by the physical properties of the matrix and the factors of temperature and pressure, while considering coalification, these factors are intrinsic and not considered external factors. These physical properties are a function of physical bonding between gas and solid at the molecular level, as influenced by different functional groups, maceral compositions, and thermal maturity [20–23]. Conventional measurement methods involve isothermal adsorption experiments and are commonly used to characterize the adsorbed methane content governed by the Langmuir-like response [20]. Low-field nuclear magnetic resonance (NMR) spectroscopy is an alternative rapid, noninvasive, and nondestructive technique to characterize petrophysical the features and fluid flow properties of unconventional reservoirs [24–29]. The amplitude of T_2 spectrum (a.u.) is closely related to the number of ^{1}H protons, which increases with the mass or volume of methane gas at different pressures. Transverse relaxation times (T_2) are generally calibrated and adopted as an index to classify the total mass of methane present within the sample. Thus, NMR can be a useful method to clearly distinguish methane content in free and adsorbed states [24,30]. The reported identification of methane phases is generally based on ~ cm length coal plugs, with methane interpreted as “coal-adsorbed methane” and “porous medium confined methane” [24,31-34]. However, methane is generated in the coalification process, with significant methane stored within the micropores of the coal. Furthermore, re-injecting methane into the core plugs cannot fully re-saturate the coal due to the limited saturation time and the difficulty in re-accessing the micropores.

We address the issue of (i) rapidly assaying methane contents between (ii) free and adsorbed states by subjecting *powdered* coal to *NMR spectroscopy*, to define both methane storage conditions and maximum storage capacity. These NMR-recovered ratios of adsorbed/free-gas are compared with independent measurements from isothermal adsorption – identifying a technique to detect these ratios in organic rich rocks. We use the technique to quantify key factors influencing methane adsorption and desorption and to control the methane content under different confining pressures. Overall, this method of characterization and this delineation of conditions controlling sorption may be used to quantify the free and adsorbed methane contents at different reservoir pressures and to clearly define the methane storage capacity of coal.

2. Materials and methods

2.1. Sampling and composition

Representative samples (*S1, S2* and *S3)* were collected from the southern Junggar Basin eastern Ordos Basin and Qinshui Basin, respectively. The southern Junggar Basin contains subbituminous to high volatile bituminous coal [16], the eastern Ordos Basin contains medium volatile bituminous coal, and Qinshui Basin contains low volatile anthracite coal, three areas with economic coalbed methane production [12,35].

Table 1
Experimental scheme for NMR pressure increments and decrements.

Experimental scheme	Equilibrium pressure (MPa)					
Pressure increments	2.5	5	7.5	10	12.5	15
Pressure decrements	12.5	10	7.5	5	2.5	

The block samples were collected from underground mine faces from the three basins with three sub-samples crushed to #60–#80 mesh size (0.180–0.250 mm). The resulting powder was vacuum-dried in an oven at 65 °C for 12 h. These three sub-sets of powdered samples for each coal type were analyzed in this study – one each for maceral composition, NMR spectroscopy and isothermal adsorption experiments. The samples were subjected to proximate analysis and measured for vitrinite reflectance and maceral composition according to Chinese Industry Standards GB/T 6948-2008, GB/T 15224.1-2018 and GB/T 8899-2013.

2.2. NMR spectroscopy under pressure

2.2.1. Experimental setup

Fig. 1 illustrates the experimental setup consisting of an NMR measurement apparatus and a volumetric sorption cell. The sample cell was both non-magnetic and non-metallic for the segment located in the magnet coil. The NMR apparatus was a MiniMR-60 NMR spectrometer, manufactured by Niumag Corporation Ltd, China. The instrument used a frequency of 23.15 MHz and a magnetic field strength of 0.54 T with a magnet coil diameter of 60 mm. The magnetic uniformity is as low as 30 ppm, in which relaxation from gas diffusion can be ignored. As a standard sequence for measuring T_2, the Carr-Purcell-Meiboom-Gill (CPMG) sequence was used in this study. The parameters were chosen to maximize the information acquired for the given samples with CPMG sequences of 18,000 echoes used. The number of scans (NS) and echo time (TE) for the NMR experiment were 16 and 0.15 ms, respectively. The temperature of the spectrometer and the analyzed samples were held constant at 22 ± 0.5 °C.

2.2.2. Experimental procedures

Experiments were run for adsorption and then desorption with balancing pressures of 2.5, 5, 7.5, 10, 12.5 and 15 MPa selected (Table 1). At each set pressure, the sample cavity was probed with the NMR at a constant sampling rate until full adsorption was attained (no change in signal). The resulting NMR T_2 spectrum of methane was then

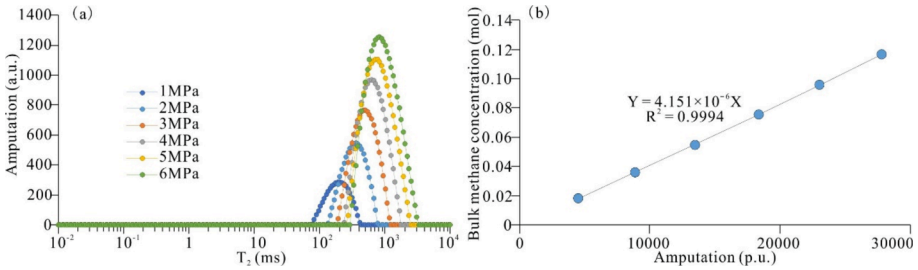

Fig. 2. Relaxation properties of bulk methane. (a) NMR measurements for bulk methane at different pressures; (b) relationship between NMR signal integrated amplitudes and specific density of bulk methane.

Table 2
Bulk methane characteristics measured by NMR.

Pressure (MPa)	Amplitude of T_2 spectrum (a.u.)	Amount of substance (mol)	Mass (g)	Concentration (mg/cm^3)
1.02	4519.162	0.018	0.291	6.699
1.99	8886.552	0.036	0.578	13.293
2.97	13462.575	0.055	0.879	20.194
4.01	18337.966	0.075	1.206	27.706
5.00	23033.776	0.096	1.530	35.175
6.00	27758.525	0.116	1.864	42.831

Note: The reference cell volume is 43.51 cm^3.

used to analyze the dynamic evolution of the signal for each balancing pressure.

2.2.3. Bulk methane property measurement

The magnitude of nuclear magnetic resonance is closely related to the number of hydrogen nuclei (1H) [36,37]. A linear relationship between T_2 and fluids in porous media has been established for NMR data as [38],

$$\frac{1}{T_2} = \mathrm{F_S}\frac{\rho}{\mathrm{r}} \tag{1}$$

$$\mathrm{r} = \mathrm{CT_2} \tag{2}$$

where, ρ is the surface relaxation rate, μm/ms; r is the pore radius, μm; and F_s is the geometric factor. The parameter F_s is 3 for spherical pores and 2 for cylindrical/tubular pores, and C is a constant. The relaxation of adsorbed methane in diffusion pores is fast due to surface relaxation [32]. Surface relaxation occurs at the pore interface and is tied to the specific surface areas. In a uniform magnetic field, the effect of diffusion relaxation is negligible [25,32].

To identify the free methane within the coal, it is necessary to correct for the relaxation properties of bulk methane (Fig. 2 and Table 3). The bulk methane peak is unimodal under all pressures, indicating that the methane is in a single state [39]. The T_2 spectra have a distinct peak at approximately 80–3000 ms, shifting to higher T_2 values with increasing pressure. The methane relaxation is mainly of spin–spin. Thus, with increasing pressure, the average free path of methane molecules decreases, resulting in an increase in the methane T_2 [40,41]. A clear linear relationship between the signal integrated amplitude and methane density is defined by data fitting together with the equation of state for the gas (Fig. 2-b).

Based on the various methane relaxation spectra, the mass of free methane under different equilibrium pressures was recorded (Table 2). By substituting the signal integrated amplitude, the mass of methane under standard conditions can be obtained as

$$N = 4.151 \times 10^{-6} A,\ R^2 = 0.9994 \tag{3}$$

where N, is the mass of methane, mol; and A, is the NMR signal integrated amplitudes.

2.2.4. Calculation of free and adsorbed methane content

The adsorbed and free methane volumes can be quantified from the signal integrated amplitude according to Eqs. (1) and (2). The relationship between the volume of adsorbed/free methane and the integrated amplitudes is determined from the T_2 spectrum under the different equilibrium pressures as:

$$V_{\mathrm{total}} = 1000 \times \mathrm{V_m} \times N \tag{4}$$

$$\begin{aligned} V_{\mathrm{total}} &= 4.151 \times 10^{-6} \times 22.4 \times 1000 \left(A_{\mathrm{adsorption}} + A_{\mathrm{free}}\right) \\ &= 0.09298 \left(A_{\mathrm{adsorption}} + A_{\mathrm{free}}\right) \end{aligned} \tag{5}$$

$$V_{\mathrm{adsorption}} = 0.09298\, A_{\mathrm{adsorption}} \tag{6}$$

$$V_{\mathrm{free}} = 0.09298\, A_{\mathrm{free}} \tag{7}$$

where V is the methane volume under standard conditions cm^3. V_{total}, $V_{\mathrm{adsorption}}$, and V_{free} are the total methane volume, adsorbed methane volume (cm^3) and free methane volume, respectively. $\mathrm{V_m}$ is the molar volume of gas, 22.4 L/mol. A is the total area under the curve of T_2 vs amplitude from the NMR. $A_{\mathrm{adsorption}}$ and A_{free} represent the area under the curve for adsorbed and free methane, respectively.

2.3. Isothermal methane adsorption experiments

2.3.1. Experimental set up

The adsorption isotherms for methane were determined by the static volumetric method (SY/T 6132–2013) and measured using an automatic adsorption system (Beishide, China). The experimental temperature was initially set at 22 °C, with the pressure increasing to a maximum adsorption pressure of 10 MPa. For each sample, adsorption was measured between 9 and 11 pressure equilibrium points, allowing at least 2 h at each pressure point until the pressure variation was<0.0003 MPa/min.

2.3.2. Correction for absolute adsorption capacity of methane

Generally, the measured mass of methane adsorbed in isothermal adsorption experiments is referred to as the excess adsorption amount. We convert this to absolute adsorption amount as [42]:

$$n_{ex} = n_{abs}(1 - \rho_g/\rho_a) \tag{8}$$

where n_{ex} and $\mathrm{n_{abs}}$ are the excess adsorption and absolute adsorption concentrations, respectively, mmol/g; ρ_a is the density of the adsorbed phase of methane, g/cm^3, $\rho_g = Mp/RT$; M is the molar mass of the adsorbent, g/mol; p is the test pressure, MPa; R is the ideal gas constant, J/(mol • K^{-1}); and T is the temperature, K.

Thermodynamic expansion is a common phenomenon in any fluid (provided that the adsorbed phase can be considered a special kind of fluid) [43-45], and must be accommodated to correct our results for temperature, as [46]:

Table 3
Proximate analysis and maceral composition analysis of the three samples.

Sample	R_o (%)	M_{ad} (%)	A_{ad} (%)	V_{ad} (%)	F_{Cad} (%)	*Vit.* (%)	*Iner.* (%)	*Lip.* (%)	*Min.* (%)
S1	0.81	0.43	12.15	33.60	53.82	60.63	36.99	11.08	1.30
S2	1.70	5.71	13.12	20.14	61.03	70.44	25.60	/	3.96
S3	3.61	3.40	12.97	3.69	79.94	69.70	27.60	/	2.70

R_o, vitrinite reflectance; M_{ad}, moisture content, air dry basis; A_{ad}, ash yield, air dry basis; V_{ad}, volatile matter, air dry basis; F_{Cad}, fixed carbon content; *Vit*, Vitrinite; *Iner*, Inertinite; *Lip*: Liptinite; *Min*, mineral.

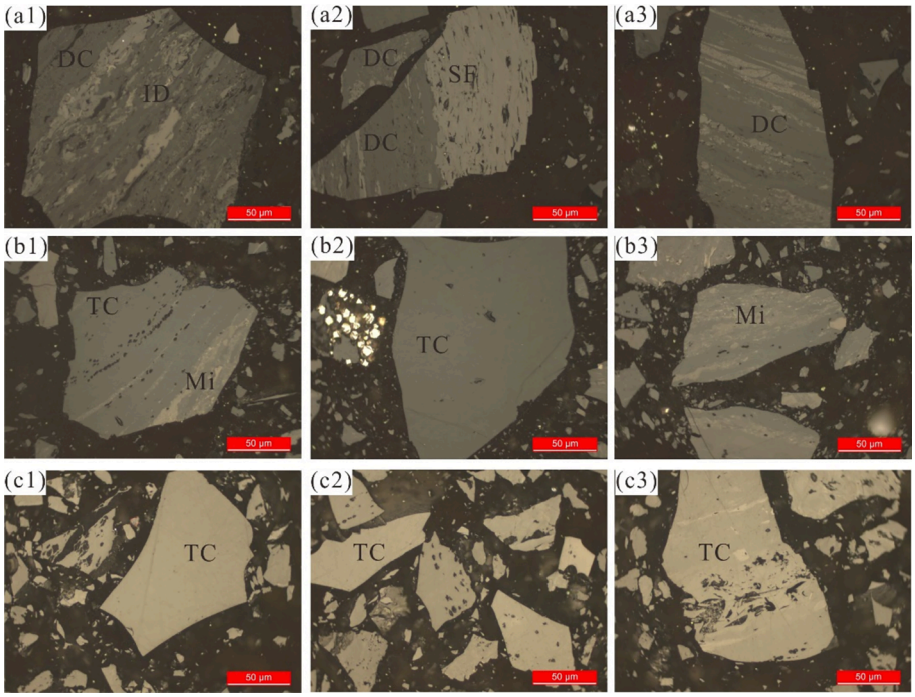

Fig. 3. Images of macerals of three coal samples. (a) *S1* (high volatile bituminous coal); (b) *S2* (low volatile bituminous coal); (c) *S3* (low volatile anthracite coals). DC, collodetrinite; ID, inertodetrinite; SF, semifusinite; Mi, macrinite; and TC, collotelinite.

$$\rho_a = \rho_b exp[\lambda \times (T - T_b)] \quad (9)$$

where ρ_b is the liquid methane density at its boiling point, 0.42236 g/cm^3; T_b is the boiling temperature of methane, 111.66 K [47]; and λ is the thermodynamic expansion coefficient, K^{-1}, $\lambda = 2.5 \times 10^{-3}$ K^{-1}.

3. Results and discussion

3.1. Studied samples

The three representative coal samples from each of the three basins have maximum vitrinite reflectance of 0.81%, 1.70% and 3.65%, effectively representing high volatile bituminous coal, low volatile bituminous coal and low volatile anthracite coal, respectively (Table 3). Maceral compositions all principally comprise vitrinite and inertinite, with sub-maceral compositions mainly of telinite, inertodetrinite and micrinite (Fig. 3). Vitrinite comprises > 60% of the maceral compositions in each of the three samples, with liptinite 11.08% for the relatively low rank sample *S1*. The fixed carbon content is higher than 45% for each of the samples, indicating sufficient potential for methane adsorption.

3.2. Discriminating between free and adsorbed methane content

3.2.1. Relaxation properties of methane in coals

Compared with the relaxation spectra of bulk methane (Fig. 2-a), the T_2 distributions and integrated amplitudes of methane within coal are distinctly different. The methane relaxation spectra exhibit four different peaks, P1, P2, P3, and P4 in Fig. 4. As the dry, methane-free coal signals has been eliminated, the four peaks are related entirely to the relaxation of methane.

The P_4 peaks are all centered near the T_2 range of 100 to 3000 ms in Figs. 2 and 4, indicating that the peak corresponds to bulk methane within the porous coal and cell that is mobile. The bulk methane exhibits a long relaxation time, with peaks local to 1000 ms. These results agree with those for bulk methane by Guo et al. (2007), Yao et al. (2014), and Quan et al. (2020) [24,25,32,46]. The relaxation time can be delayed by the application of an increase in pressure, with higher pressure resulting in higher amplitude and sharper peaks (Fig. 2). At elevated pressure, the molecular density increases while the free molecular path decreases, resulting in more frequent molecular interactions [21]. Thus, the relaxation time decreases as the methane pressure is increased. As the tested samples comprise powdered coal fines, the sample is rapidly saturated within the cell. The measured bulk methane content is much lower than the results recovered from cores, as reported by [25].

The T_2 spectrum of methane confined within coal porous spaces is considerably different from that measured in bulk. The methane within the coals is assumed to exist in one of three states: solid solution within the coal matrix, in the adsorbed state on the inner surfaces and within small pores, and as free gas in macropores and fractures [48,49]. The P1, P2 and P3 peaks are each attributed to the surface relaxation of methane in each of these three states (Fig. 5). The surface interaction generally corresponds to the van der Walls force and hydrogen bond between methane and coal at the pore walls or other inner surfaces [19]. The

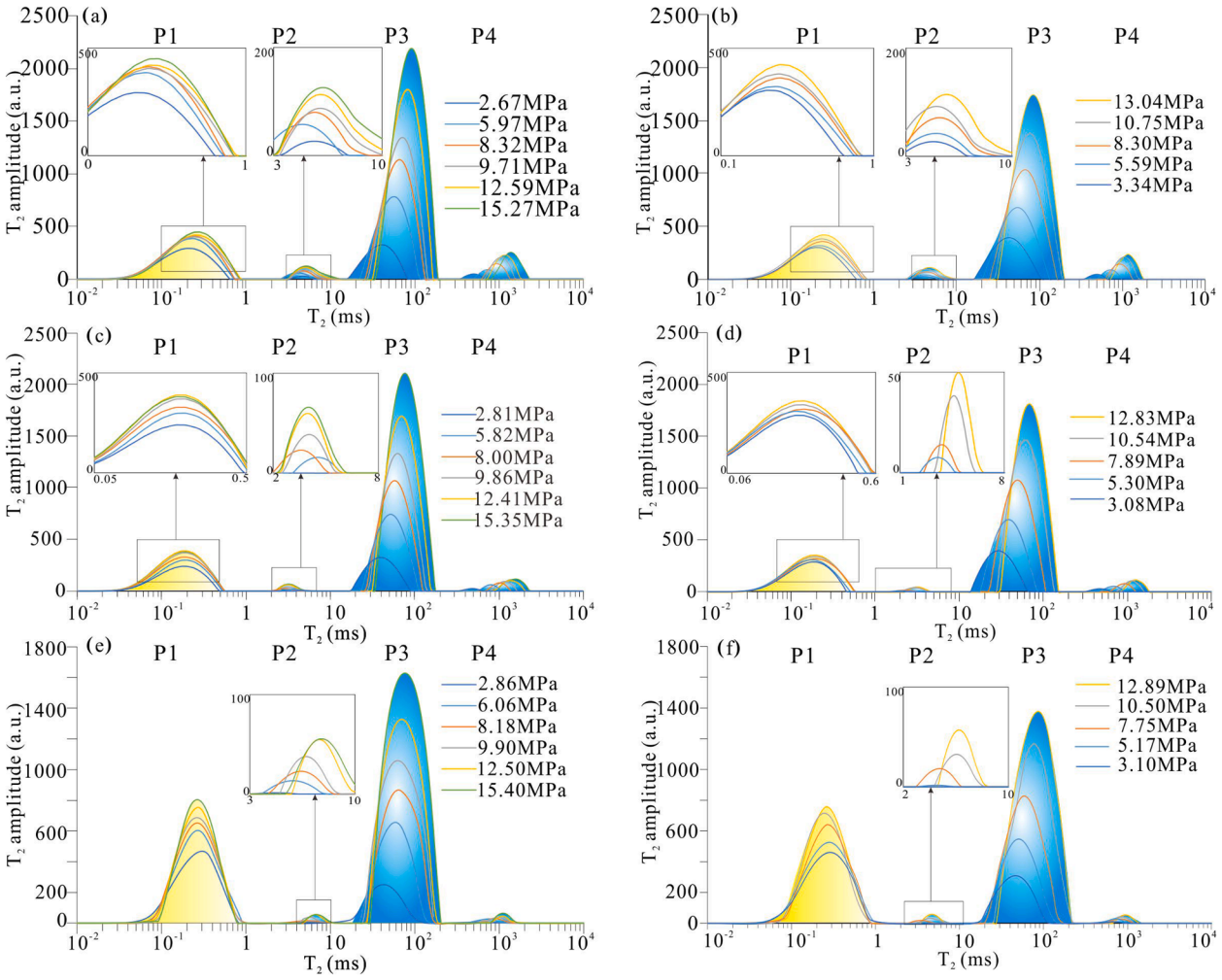

Fig. 4. T_2 spectra for adsorbed/free methane at different pressures using NMR for sample *S1*, (a) pressure increments, (b) pressure decrements; sample *S2* (c) pressure increments, (d) pressure decrements; and sample *S3* (e) pressure increments, (f) pressure decrements.

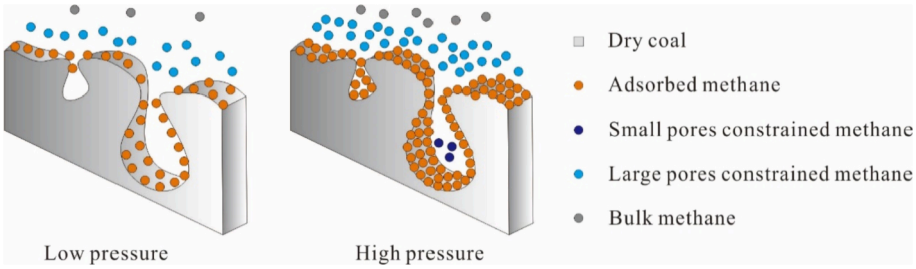

Fig. 5. Model for adsorbed methane. Methane in small pores, large pores and fractures together with bulk methane. Bulk methane, the methane in the porous coal and cell that is mobile; free methane, methane in small pores, large pores and fractures; adsorbed methane, methane on the inner surfaces of coal micropores or within the coal matrix.

molecular dynamics of methane, e.g., molecular tumbling, were hindered [27].

Previous research has shown that protons in smaller pores with high surface to volume (S/V) ratios exhibit a slower relaxation than those in larger pores and fractures. Thus, the P1 peak (i.e. 0.01–1 ms) corresponds to methane on the inner surfaces of coal micropores or within the coal matrix. Peak P2 reflects the response to free-gas methane in small pores and P3 to that in large pores and fractures. The P2 peak is at ~ 2 to 20 ms, representing an unstable state part way between adsorbed and free states - likely reflecting constrained methane in small pores of very limited radius. This unstable condition is also reflected in the variation in the peak axis which differs from the increase in relaxation time of the bulk methane due to a pressure increase. The P3 peak, located between the T_2 distribution of ~ 20 and 1000 ms, also shows a longer relaxation time as pressure is increased. This represents methane in the free-state but constrained in large pores or fractures. Prior studies were limited to a maximum methane pressure of 7 MPa, while our experiments could probe to15 MPa. This higher spectrum of probed pressures shows that the observed states are either in accordance with former results, such as for bulk methane [24,25], or consistent with the variations in relaxation time, e.g., methane constrained in small pores, large pores or fractures.

Table 4
T_2 spectra and methane concentrations for pressure-increment and -decrement experiments using NMR at different equilibrium pressures.

Sample		Experimental scheme (MPa)	Equilibrium pressure (MPa)	T_2 amplitude (a.u.)		Methane concentration (m^3/t)	
				Adsorbed methane	Free methane	Adsorbed methane	Free methane
S1	Pressure increment	2.5	2.67	7034.83	5294.16	20.33	15.30
		5.0	5.97	9247.78	12581.17	26.72	36.35
		7.5	8.32	10116.04	18364.57	29.23	53.06
		10.0	9.71	10113.14	22247.34	29.22	64.28
		12.5	12.59	10667.22	29777.23	30.82	86.04
		15.0	15.27	11052.09	36825.20	31.93	106.40
	Pressure decrement	12.5	13.05	10153.56	31782.74	29.34	91.83
		10	10.75	9472.89	25444.79	27.37	73.52
		7.5	8.30	8609.83	18978.87	24.88	54.84
		5.0	5.59	7754.87	12297.97	22.41	35.53
		2.5	3.34	6994.41	7115.18	20.21	20.56
S2	Pressure increment	2.5	2.81	5314.93	4997.67	14.41	13.55
		5.0	5.82	6666.72	11110.16	18.07	30.12
		7.5	8.00	7688.45	15932.66	20.84	43.19
		10.0	9.86	8393.08	20106.95	22.75	54.51
		12.5	12.41	8834.19	26101.07	23.95	70.76
		15.0	15.35	8880.30	33239.59	24.07	90.11
	Pressure decrement	12.5	12.83	8362.59	27656.85	22.67	74.97
		10	10.54	7939.86	22058.75	21.52	59.80
		7.5	7.89	7530.11	15893.93	20.41	43.09
		5.0	5.30	6988.76	10303.08	18.95	27.93
		2.5	3.08	6205.79	5853.21	16.82	15.87
S3	Pressure increment	2.5	2.86	10720.20	4425.50	26.90	11.10
		5.0	6.06	12105.34	11209.83	30.37	28.13
		7.5	8.18	12960.74	15956.81	32.52	40.04
		10.0	9.9	13387.80	19753.79	33.59	49.56
		12.5	12.5	14090.55	25511.84	35.35	64.01
		15.0	15.4	14449.81	32058.59	36.25	80.43
	Pressure decrement	12.5	12.89	14021.95	26711.04	35.18	67.02
		10	10.5	13577.60	21177.52	34.07	53.13
		7.5	7.75	12784.06	15015.87	32.08	37.67
		5.0	5.17	11866.05	9509.89	29.77	23.86
		2.5	3.10	10484.41	5343.57	26.31	13.41

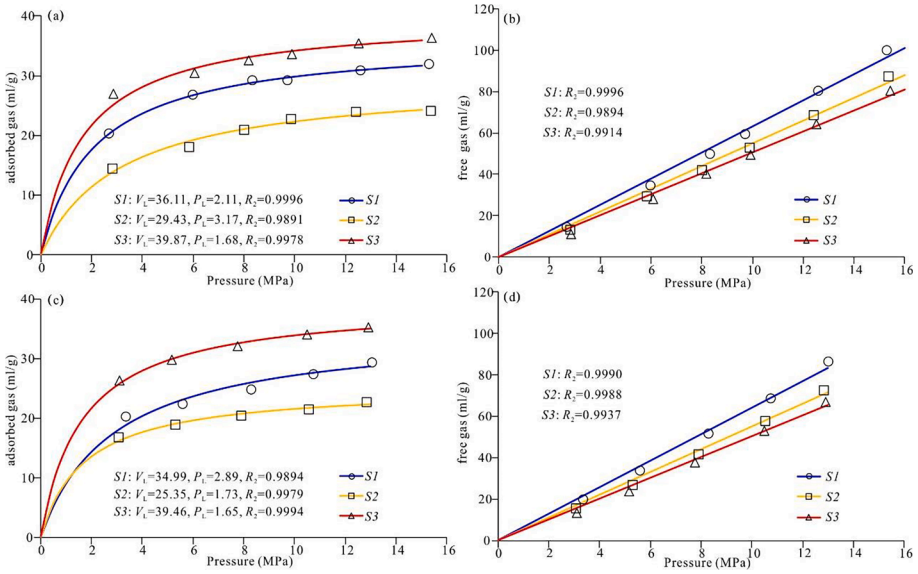

Fig. 6. Methane concentration for adsorbed and free methane at different pressures using NMR. (a) Adsorbed methane in pressure increments; (b) free methane in pressure increments; (c) adsorbed methane in pressure decrements; and (d) free methane in pressure decrements.

3.2.2. Variation in free and adsorbed methane content with pressure variation

The volumes of adsorbed/free methane under different equilibrium pressures are quantitatively estimated from the T_2 spectrum (Eqs. (4)–(7), Table 4). The adsorbed methane concentrations gradually increase with an increase in pressure, from 20.33 m^3/t to 31.93 m^3/t as we transit from 2.5 MPa to 15 MPa in sample *S1* (Fig. 6-a). A similar increase is recorded for sample *S2* of 14.41 m^3/t to 24.07 m^3/t over the same pressure range, and sample *S3* of 26.90 m^3/t to 36.25 m^3/t over the same pressure range. During pressure decreases, the methane content generally recovers to the initial conditions, ~20.21 m^3/t, 16.82 m^3/t and 26.31 m^3/t at 2.5 MPa for samples *S1*, *S2* and *S3*, respectively (Fig. 6-c).

The free methane content shows a much wider range of variation than the adsorbed methane content (Fig. 6- b and d). The free methane

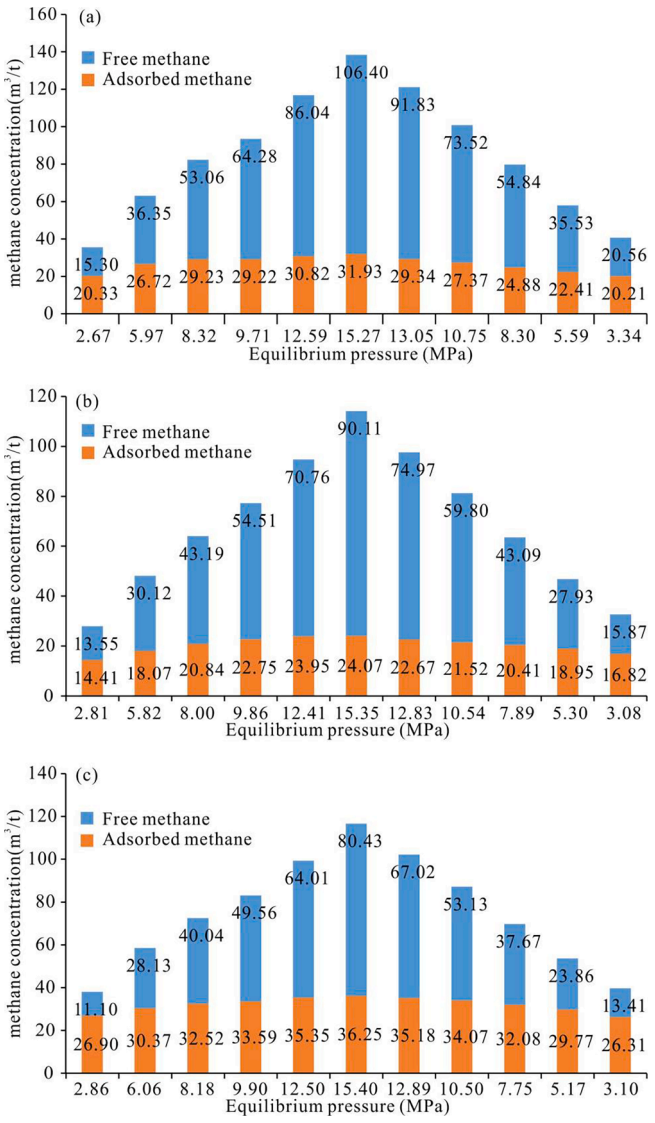

Fig. 7. Concentration of adsorbed and free methane at different equilibrium pressures using NMR. (a) Sample *S1*; (b) Sample *S2* and (c) Sample *S3*.

in *S1* increases from 14.40 m^3/t at 2.67 MPa to 99.95 m^3/t at 15.27 MPa during pressure increases, indicating a seven-fold increase (Fig. 6-b). During a decrease in pressure the methane content decreases to 19.66 m^3/t at 3.34 MPa (Fig. 6-d). A positive linear relationship between the free methane content and the equilibrium pressure is apparent (Table 4, Fig. 6-b and d).

At the initial 2.5 MPa during pressure increases, the adsorbed methane content is higher than the free methane content for all three samples (Fig. 6-a and b). At > 5 MPa, the free methane content is higher than the adsorbed methane content in samples *S1* and *S2*. The free/adsorbed methane ratios of the three samples range 0.75–3.33, 0.94–3.74 and 0.41–2.22 from ~ 2.5 MPa to ~ 15 MPa for samples *S1*, *S2* and *S3* (Fig. 7). The higher pressures result in a continuous increase in methane content.

3.3. Adsorption and desorption processes

The details of the adsorption and desorption processes at each equilibrium pressure are recorded by the T_2 signal amplitude (Fig. 8). In both the adsorption and desorption processes the balance time is generally ~ 40–60 min. The integrated T_2 amplitudes increase/decrease rapidly during the first 20-minutes and then increase/decrease slowly

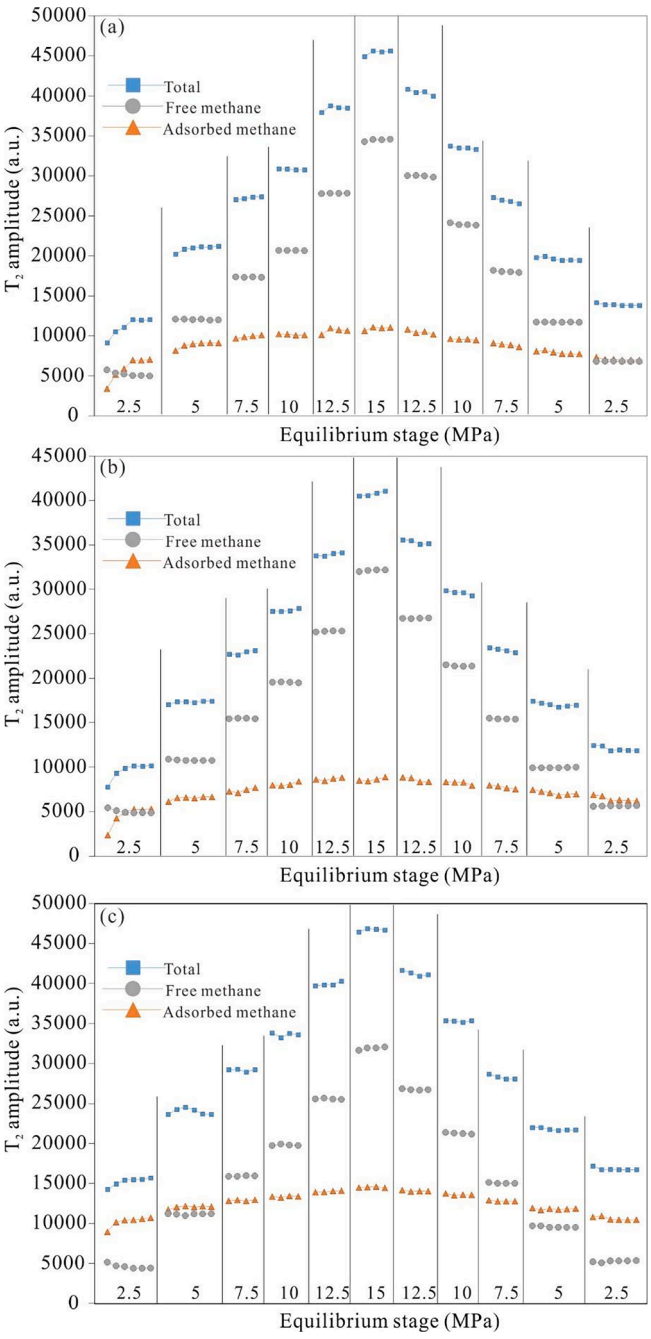

Fig. 8. T_2 amplitude for adsorbed/free methane at different equilibrium pressures using NMR. Test interval for each point is ~ 20 mins at each equilibrium pressure. (a) Sample *S1*; (b) Sample *S2* and (c) Sample *S3*.

over the remaining 20-minutes. Sample *S2* is selected in the following section for a detailed illustration of adsorption and desorption processes under each equilibrium pressure (Figs. 8 and 9).

With increasing pressure, the balanced pressure decreases during each equilibrium stage. For sample *S2*, the final balanced pressure decreases from 3.01 MPa to 2.81 MPa, indicating that methane is adsorbed (Fig. 9). For higher balance pressures (~7.5 MPa to ~ 15 MPa), a rapid equilibrium state is reached with little subsequent variation in adsorbed and free methane ratios (Figs. 8 and 9). The total mass/number of methane molecules remains constant during the balancing process under each equilibrium pressure; thus, free methane is gradually transformed into the adsorbed state. For pressures under 5 MPa, the coal matrix retains sufficient sorption capacity to further adsorb methane as

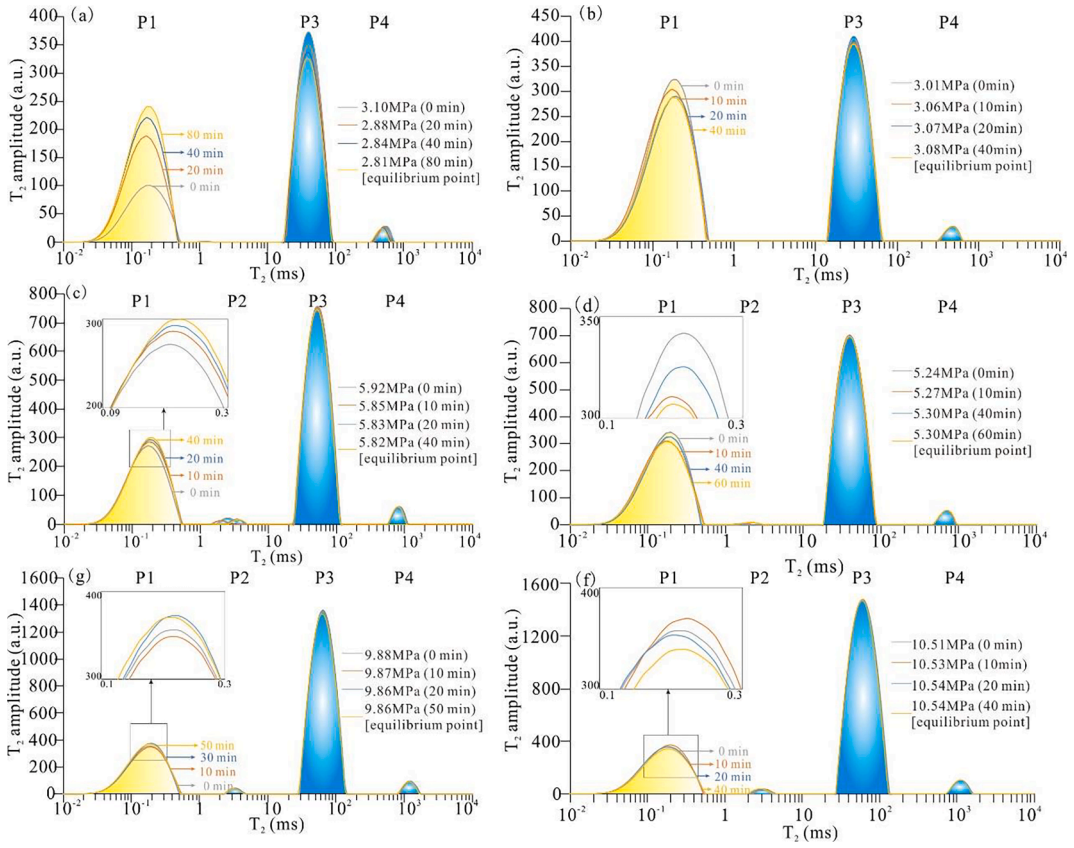

Fig. 9. T_2 spectra for adsorbed/free methane at different equilibrium pressures using NMR for *S2*. (a) 2.5 MPa stage of pressure increment, (b) 2.5 MPa stage of pressure decrement, (c) 5 MPa stage of pressure increment, (d) 5 MPa stage of pressure decrement, (e) 10 MPa stage of pressure increment, and (f) 10 MPa stage of pressure decrement.

the pressure balances.

At pressures of 12.5 and 15 MPa, the adsorbed methane content fluctuates under equilibrium pressure, indicating methane exchange between adsorption and desorption states (Fig. 8). As the pressure is decreased, adsorbed methane gradually transforms to free methane. Both adsorbed and free methane show little fluctuation when decreased to a threshold equilibrium pressure. The final adsorbed methane content is nearly equivalent to the maximum adsorbed methane at the initial ~ 2.5 MPa (Fig. 9).

3.4. Isothermal methane adsorption

The methane adsorption isotherms at different pressures are shown in Fig. 10 and Table 5. As expected, methane adsorption for all coal samples shows a large initial increase with a pressure increase that subsequently decreases. The V_L values for the three samples are 26.47, 17.84 and 28.81 m^3/t, respectively. The absolute adsorption isotherms under different pressures are obtained from Eqs. (8) and (9), with simulated values of V_L of 38.23 and 27.34 m^3/t. Apparent from Fig. 10, the absolute adsorption concentrations also show a rapid initial increase, after which the rate of increase declines. When gas pressure is low (0–5 MPa), the excess adsorption is near-equivalent to the absolute adsorption volume. This is mainly because, when gas pressure is low, the gas volume phase density is relatively small and the volume in the adsorbed phase is negligible [45]. If the excess adsorption curve at low pressure is used to directly evaluate the adsorbed content in reservoirs, it will significantly underestimate the actual adsorption capacity [42].

3.5. Validation – NMR -versus- isothermal adsorption measurements

Comparing the results of the three samples, the adsorption capacity shows the same trend with increasing pressure. The change in the measured adsorbed methane volume with gas pressure is fit to a Langmuir isotherm and the Langmuir adsorption parameters, i.e. the Langmuir pressure (V_P) and Langmuir volume (V_L), and recovered. The calculated V_L values for samples *S1*, *S2* and *S3* using NMR in the pressure increase experiments are 36.11, 29.43 and 39.87 m^3/t, respectively (Table 6). The V_L values from the absolute adsorption curves are 38.23, 27.34 and 40.63 m^3/t, respectively, representing good agreement with the NMR results.

It should be noted that the results show a better fit at low pressures. When the gas pressure is low, the gas volume phase density is relatively small and the coal retains a finite remaining potential to adsorb excess free methane. These results further confirm that the NMR results represent absolute adsorption methane contents.

For porous solids, excess adsorption may be converted to absolute adsorption via calculation. For low pressure, it is convenient to treat excess adsorption as absolute adsorption when the two quantities are equal within the accuracy of the measurements. At high pressure, the excess variables are meaningless. The difference between the absolute adsorption capacity and the excess adsorption capacity increases with the increasing pressure, and the excess adsorption capacity calculated from the isotherm adsorption data cannot reflect the true adsorption capacity. Many properties of the adsorbed phase depend on the absolute amount, but not on the excess adsorption.

Presently, there are no direct methods to obtain absolute adsorbed methane contents [50–52]. A simple method to determine the absolute adsorption based on NMR is proposed by the authors. The absolute adsorption curve is in good agreement with the NMR results. As a non-destructive analysis technique, NMR spectroscopy can also quantitatively identify methane in all of its multiphase states, a feature not available for isothermal adsorption measurements and here available for

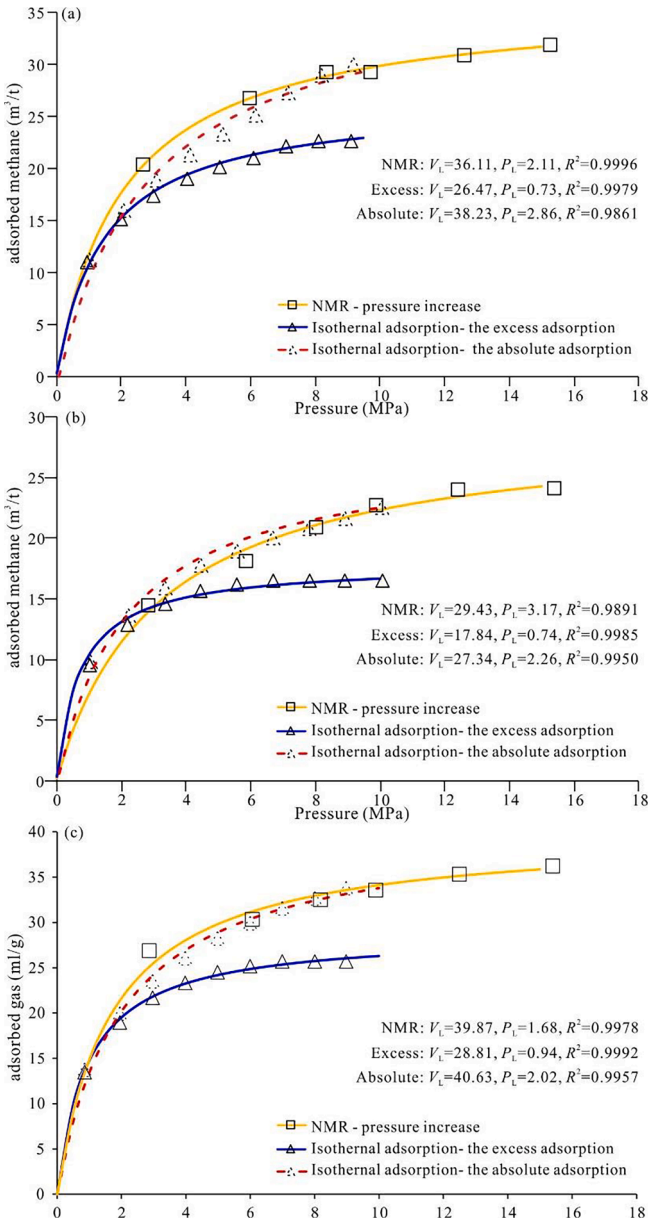

Fig. 10. Comparison of adsorbed methane from isothermal adsorption and NMR results at different pressures. (a) Sample *S1*; and (b) Sample *S2*.

reservoir pressures > 10 MPa.

4. Conclusions

We developed an NMR spectroscopy protocol to measure the relative and absolute mass of free and adsorbed methane and compared these characterizations with adsorption measurements from isothermal experiments. The accuracy of the testing method was confirmed, and the following conclusions were reached:

(1) T_2 spectra for bulk methane and methane saturated coal powders enable the masses of adsorbed methane (P1), free methane (P2 and P3) and bulk methane (P4) to be acquired. Beyond this, the free methane may be classified as inhabiting either small pores (P2) or large pores (P3). The P1, P2, P3 and P4 peaks in the T_2 spectra correspond to windows of 0.01–1, 1–20, 20–100, and ~ 1000 ms, respectively and define the storage habit of methane.

(2) Free and adsorbed gas contents at equilibrium pressures from 0 to 15 MPa can be readily quantified. The free methane content is lower than the adsorbed methane content at < 5 MPa, while the free methane content is generally dominant at > 5 MPa. The adsorbed methane content plateaus at its maximum value at ~ 10 MPa, regardless of the free gas content continuously increases at > 10 MPa.

(3) High confining pressures result in more rapid adsorption–desorption equilibria than at low pressure conditions. Below a pressure of 5 MPa the adsorbed methane content gradually increases with a consequent decrease in free methane. Adsorbed and free methane quickly reach their balanced condition under high pressures, and the exchange between adsorbed and desorbed states can be observed.

Table 6
Comparison among fits to Langmuir adsorption parameters.

Fit parameters and fit quality	*S1*		*S2*		*S3*	
	V_L(m^3/t)	P_L(MPa)	V_L(m^3/t)	P_L(MPa)	V_L(m^3/t)	P_L(MPa)
NMR result	36.11	2.11	29.43	3.17	39.87	1.68
Methane isothermal adsorption-the excess adsorption	26.47	0.73	17.84	0.74	28.81	0.94
Methane isothermal adsorption-the absolute adsorption	38.23	2.86	27.34	2.26	40.63	2.02

V_L, Langmuir volume; m^3/t, P_L, Langmuir pressure, MPa.

Table 5
Excess and absolute adsorbed methane concentration for isothermal methane adsorption.

S1			*S2*			*S3*		
Pressure (MPa)	Excess adsorbed methane (m^3/t)	Absolute adsorbed methane (m^3/t)	Pressure (MPa)	Excess adsorbed methane (m^3/t)	Absolute adsorbed methane (m^3/t)	Pressure (MPa)	Excess adsorbed methane (m^3/t)	Absolute adsorbed methane (m^3/t)
0.93	10.94	11.19	1.02	9.57	9.81	0.86	13.47	13.75
1.99	15.12	15.93	2.2	12.85	13.62	1.95	18.96	19.95
3.01	17.36	18.84	3.33	14.52	15.90	2.97	21.7	23.52
4.04	19.01	21.27	4.44	15.68	17.76	3.98	23.34	26.07
5.06	20.15	23.26	5.56	16.14	18.93	4.99	24.52	28.254
6.07	21.04	25.08	6.67	16.48	20.03	6	25.17	29.94
7.08	22.12	27.27	7.79	16.48	20.80	7	25.69	31.57
8.11	22.68	28.94	8.91	16.48	21.63	8.01	25.69	32.67
9.1	22.68	29.96	10.04	16.48	22.53	8.98	25.69	33.80

(4) Adsorbed methane contents acquired by NMR and isothermal adsorption experiment show good consistency. The NMR results can directly give the absolute adsorbed methane content, which can be beneficial in clearly discriminating the methane distribution within coal in different environments.

Declaration of Competing Interest

The authors declare that they have no known competing financial interests or personal relationships that could have appeared to influence the work reported in this paper.

Acknowledgment

This study was supported by the National Natural Science Foundation of China (Grant No. 42072194, U1910205), the Fundamental Research Funds for the Central Universities (800015Z1190, 2021YJSDC02). We would like to thank Haitao Hu and Dr. Shuai Hua for their help in carrying out the experiments.

References

[1] J. Li, S. Lu, P. Zhang, J. Cai, W. Li, S. Wang, W. Feng, Estimation of gas-in-place content in coal and shale reservoirs: a process analysis method and its preliminary application, Fuel 259 (2020) 116266, https://doi.org/10.1016/j.fuel.2019.116266.
[2] Y. Li, D. Cao, P. Wu, X. Niu, Y. Zhang, Variation in maceral composition and gas content with vitrinite reflectance in bituminous coal of the eastern Ordos basin, China. J. Pet. Sci. Eng. 149 (2017) 114–125.
[3] C. Peng, C. Zou, T. Zhou, K. Li, Y. Yang, G. Zhang, W. Wang, Factors affecting coalbed methane (CBM) well productivity in the Shizhuangnan block of southern Qinshui basin, North China: investigation by geophysical log, experiment and production data, Fuel 191 (2017) 427–441.
[4] S. Zhi, D. Elsworth, The role of gas desorption on gas outbursts in underground mining of coal, Geomech. Geophys Geo-energ. Geo-resour. 2 (3) (2016) 151–171.
[5] T.A. Moore, Coalbed methane: a review, Int. J. C. Geol. 101 (2012) 36–81.
[6] Z. Wang, W. Su, X. Tang, J. Wu, Influence of water invasion on methane adsorption behavior in coal, Int. J. Coal Geol. 197 (2018) 74–83.
[7] Y. Li, Y. Wang, J. Wang, Z. Pan, Variation in permeability during CO2–CH4 displacement in coal seams: part 1 – experimental insights, Fuel 263 (2020) 116666.
[8] P. Massarotto, S.D. Golding, J.-S. Bae, R. Iyer, V. Rudolph, Changes in reservoir properties from injection of supercritical CO2 into coal seams—a laboratory study, Int. J. Coal Geol. 82 (3-4) (2010) 269–279.
[9] G.K.W. Dawson, S.D. Golding, P. Massarotto, J.S. Esterle, Experimental supercritical CO_2 and water interactions with coal under simulated in situ conditions, Energy Procedia 4 (2011) 3139–3146.
[10] K. Czerw, Methane and carbon dioxide sorption/desorption on bituminous coal—experiments on cubicoid sample cut from the primal coal lump, Int. J. Coal Geol. 85 (1) (2011) 72–77.
[11] Y. Li, D. Tang, P. Wu, X. Niu, K. Wang, P. Qiao, Z. Wang, Continuous unconventional natural gas accumulations of Carboniferous-Permian coal-bearing strata in the Linxing area, northeastern Ordos basin, China, J. Nat. Gas Sci. Eng. 36 (2016) 314–327.
[12] Y. Li, J. Yang, Z. Pan, S. Meng, K. Wang, X. Niu, Unconventional natural gas accumulations in stacked deposits: a discussion of Upper Paleozoic coal-bearing strata in the east margin of the Ordos Basin, China, Acta Geologica Sinica (English Edition) 93 (1) (2019) 111–129.
[13] P.K. Singh, Geological and petrological considerations for CBM exploration: a review, Energy Sources Part A 33 (2011) 1211–1220.
[14] D.K. Murray, Coal bed methane; natural gas resources from coal seams, in: D. C. Peters (Ed.), Geology Ž .in Coal Resource Utilization, Tech Books, United States, 1991, pp. 97–103.
[15] R.M. Bustin, C.R. Clarkson, Geological controls on coalbed methane reservoir capacity and gas content, Int. J. Coal Geol. 38 (1-2) (1998) 3–26.
[16] Y. Li, C. Zhang, D. Tang, Q. Gan, X. Niu, K. Wang, R. Shen, Coal pore size distributions controlled by the coalification process: an experimental study of coals from the Junggar, Ordos and Qinshui basins in China, Fuel 206 (2017) 352–363.
[17] C.J. Zhu, J. Ren, J.M. Wan, Methane adsorption on coals with different coal rank under elevated temperature and pressure, Fuel 254 (2019), 115686.
[18] J. Milewska-Duda, J. Duda, A. Nodzeński, J. Lakatos, Absorption and adsorption of methane and carbon dioxide in hard coal and active carbon, Langmuir 16 (12) (2000) 5458–5466.
[19] S. Kędzior, Accumulation of coalbed methane in the south-west part of the Upper Silesian Coal Basin (southern Poland), Int. J. Coal Geol. 80 (1) (2009) 20–34.
[20] R.M. Flores, Coal and Coalbed Gas, Fueling the Future, Elsevier Science, Waltham, 2014.
[21] P.K. Singh, P.K. Rajak, V.K. Singh, M.P. Singh, A.S. Naik, S.V. Raju, Studies on thermal maturity and hydrocarbon potential of lignites of Bikaner-Nagaur basin, Rajasthan, Energy Explor. Exploit. 34 (1) (2016) 140–157.
[22] P.K. Singh, Geological and petrological considerations for CBM exploration: a review, Energy Sources Part A: Recovery, Utilization, and Environmental Effects. Taylor & Francis 33 (2011) 1211–1220.
[23] K. Mosher, J. He, Y. Liu, E. Rupp, J. Wilcox, Molecular simulation of methane adsorption in micro- and mesoporous carbons with applications to coal and gas shale systems, Int. J. Coal Geol. 109-110 (2013) 36–44.
[24] R. Guo, D. Mannhardt, A. Kantzas, Characterizing moisture and gas content of coal by low-field NMR, J. Can. Pet. Technol. 46 (10) (2007) 49–54.
[25] Y. Yao, D. Liu, S. Xie, Quantitative characterization of methane adsorption on coal using a low-field NMR relaxation method, Int. J. Coal Geol. 131 (2014) 32–40.
[26] D. Liu, H. Ge, J. Liu, Y. Shen, Y. Wang, Q. Liu, C. Jin, Y. Zhang, Experimental investigation on aqueous phase migration in unconventional gas reservoir rock samples by nuclear magnetic resonance, J. Nat. Gas Sci. Eng. 36 (2016) 837–851.
[27] B. Pandey, D.B. Pathak, N. Mathur, A.K. Jaitly, A.K. Singh, P.K. Singh, A preliminary evaluation on the prospects of hydrocarbon potential in the carbonaceous shales of Spiti and Chikkim formations, Tethys Himalaya, India, J Geol. Soc. India. 92 (4) (2018) 427–434.
[28] S. Zheng, Y. Yao, D. Liu, Y. Cai, Y. Liu, Characterizations of full-scale pore size distribution, porosity and permeability of coals: a novel methodology by nuclear magnetic resonance and fractal analysis theory, Int. J. Coal Geol. 196 (2018) 148–158.
[29] A.E. Ozeni, R.F. Sigal, T1/T2 NMR surface relaxation ratio for hydrocarbons and brines in contact with mature organic-shale reservoir rocks, Petrophysics 54 (1) (2013) 11–19.
[30] R. Guo, A. Kantzas, Assessing the water uptake of Alberta coal and the impact of CO_2 injection with low-field NMR, J. Can. Pet. Technol. 48 (7) (2009) 40–46.
[31] Y. Yang, X. Li, Y. Zhang, Y. Mei, R. Ding, Insights into moisture content in coals of different ranks by low field nuclear resonance, Energ. Geos. 1 (3-4) (2020) 93–99.
[32] F. Quan, C. Wei, J. Zhang, S. Feng, S. Hao, G. Lu, Y. Hu, Study on desorption and diffusion dynamics of coal reservoir through step-by-step depressurization simulation——an experimental simulation study based on LF-NMR technology, J. Nat. Gas Sci. Eng. 75 (2020) 103149.
[33] F. Wang, Y. Yao, Z. Wen, Q. Sun, X. Yuan, Effect of water occurrences on methane adsorption capacity of coal: a comparison between bituminous coal and anthracite coal, Fuel 266 (2020) 117102.
[34] M. Lu, L.D. Connell, Z. Pan, Wetting fluid behaviour with phase transition in geological nanopores: liquid film, capillary condensation and evaporative flow, J. Pet. Sci. Eng. 195 (2020) 107570.
[35] Y. Li, Z. Wang, P. Wu, X. Gao, Z. Yu, Y. Yu, J. Yang, Organic geochemistry of Upper Paleozoic source rocks in the eastern margin of the Ordos Basin, China: input and hydrocarbon generation potential, J. Pet. Sci. Eng. 181 (2019) 106202.
[36] R.L. Kleinberg, H.J. Vinegar, NMR properties of reservoir fluids, Log. Anal. 37 (1996) 20–32.
[37] C. Morriss, D. Rossini, C. Straley, P. Tutunjian, H. Vinegar, Core analysis by low-field NMR, Log. Anal. 38 (2) (1997).
[38] R.L. Kleinberg, M.A. Horsfield, Transverse relaxation processes in porous sedimentary rock, J. Magn. Reson. 88 (1) (1990) 9–19.
[39] Z. Liu, D. Liu, Y. Cai, Y. Yao, Z. Pan, Y. Zhou, Application of nuclear magnetic resonance (NMR) in coalbed methane and shale reservoirs: a review, Int. J. Coal Geol. 218 (2020) 103261, https://doi.org/10.1016/j.coal.2019.103261.
[40] C. Straley, D. Rossini, H. Vinegar, T. Pierre, C. Morriss, Core analysis by low field NMR, Log. Anal. 38 (2) (1997) 84–93.
[41] A. Papaioannou, R. Kausik, Methane storage in nanoporous media as observed via high field NMR relaxometry, Geophysics 4 (2) (2015), 024018.
[42] Z. Jin, A. Firoozabadi, Effect of water on methane and carbon dioxide sorption in clay minerals by Monte Carlo simulations, Fluid Phase Equil. 382 (2014) 10–20.
[43] X. Luo, S. Wang, Z. Wang, Z. Jing, M. Lv, Z. Zhai, T. Han, Adsorption of methane, carbon dioxide and their binary mixtures on Jurassic shale from the Qaidam Basin in China, Int. J. Coal Geol. 150 (2015) 210–223.
[44] H. Tian, T. Li, T. Zhang, X. Xiao, Characterization of methane adsorption on overmature Lower Silurian-Upper Ordovician shales in Sichuan Basin, southwest China: experimental results and geological implications, Int. J. Coal Geol. 156 (2016) 36–49.
[45] R. Sakurovs, S. Day, S. Weir, G. Duffy, Application of a modified Dubinin Radushkevich equation to adsorption of gases by coals under supercritical conditions, Energy Fuels 21 (2) (2007) 992–997.
[46] S. Ozawa, S. Kusumi, Y. Ogino, Physical adsorption of gases at high pressure. IV. An improvement of the Dubinin-Astakhov adsorption equation, J. Colloid Interface Sci. 56 (1) (1976) 83–91.
[47] J. Li, Z. Chen, K. Wu, K. Wang, J. Luo, D. Feng, X. Li, A multi-site model to determine supercritical methane adsorption in energetically heterogeneous shales, Chem. En. J. 349 (2018) 438–455.
[48] A.D. Alexeev, E.V. Ulyanova, G.P. Starikov, N.N. Kovriga, Latent methane in fossil coals, Fuel 89 (2004) 1407–1411.
[49] A.D. Alexeev, T.A. Vasylenko, E.V. Ul'yanova, Phase states of methane in fossil coals, Solid State Commun. 130 (2004) 669–673.
[50] X. Tang, Z. Jiang, H. Huang, S. Jiang, L. Yang, F. Xiong, L. Chen, J. Feng, Lithofacies characteristics and its effect on gas storage of the Silurian Longmaxi

marine shale in the southeast Sichuan Basin, China, J. Nat. Gas Sci. Eng. 28 (2016) 338–346.
[51] S. Zhou, Y. Ning, H. Wang, H. Liu, H. Xue, Investigation of methane adsorption mechanism on Longmaxi shale by combining the micropore filling and monolayer coverage theories, Adv. Geo-Energy Res. 2 (3) (2018) 269–281.
[52] J. Singh, J. Cai, A mechanistic model for multi-scale sorption dynamics in shale, Fuel 234 (2018) 996–1014.